

The role of spartin and its novel ubiquitin binding region in DALIS occurrence

Amelia B. Karlsson^a, Jacqueline Washington^b, Valentina Dimitrova^c, Christopher Hooper^d, Alexander Shekhtman^b, and Joanna C. Bakowska^a

^aDepartment of Molecular Pharmacology and Therapeutics, Loyola University Chicago, Maywood, IL 60153;

^bDepartment of Chemistry, State University of New York at Albany, Albany, NY 12222; ^cDepartment of Physiology, University of Pennsylvania, Philadelphia, PA 19104; ^dDepartment of Oncology, University of Wisconsin–Madison, Madison, WI 53705

ABSTRACT Troyer syndrome is an autosomal recessive hereditary spastic paraplegia (HSP) caused by frameshift mutations in the *SPG20* gene that results in a lack of expression of the truncated protein. Spartin is a multifunctional protein, yet only two conserved domains—a microtubule-interacting and trafficking domain and a plant-related senescence domain involved in cytokinesis and mitochondrial physiology, respectively—have been defined. We have shown that overexpressed spartin binds to the Ile44 hydrophobic pocket of ubiquitin, suggesting spartin might contain a ubiquitin-binding domain. In the present study, we demonstrate that spartin contributes to the formation of dendritic aggresome-like induced structures (DALIS) through a unique ubiquitin-binding region (UBR). Using short hairpin RNA, we knocked down spartin in RAW264.7 cells and found that DALIS frequency decreased; conversely, overexpression of spartin increased the percentage of cells containing DALIS. Using nuclear magnetic resonance spectroscopy, we characterized spartin's UBR and defined the UBR's amino acids that are key for ubiquitin binding. We also found that spartin, via the UBR, binds Lys-63–linked ubiquitin chains but does not bind Lys-48–linked ubiquitin chains. Finally, we demonstrate that spartin's role in DALIS formation depends on key residues within its UBR.

Monitoring Editor
Sandra Lemmon
University of Miami

Received: Dec 2, 2013

Revised: Jan 28, 2014

Accepted: Jan 31, 2014

INTRODUCTION

Hereditary spastic paraplegias (HSPs) are a group of neurological disorders characterized by progressive lower-extremity weakness and spasticity (Salinas *et al.*, 2008; Blackstone, 2012). Troyer syndrome is an autosomal recessive HSP caused by frameshift mutations in the *SPG20* gene (Patel *et al.*, 2002; Manzini *et al.*, 2010). These mutations result in a lack of expression of the spartin protein,

which leads to a loss-of-function pathogenesis (Bakowska *et al.*, 2008; Manzini *et al.*, 2010). Spartin is a multifunctional protein that consists of two conserved domains—a microtubule-interacting and trafficking (MIT) domain and a plant-related senescence domain (Ciccarelli *et al.*, 2003). These domains are involved in cytokinesis and mitochondrial physiology, respectively (Renvoise *et al.*, 2010; Joshi and Bakowska, 2011). We have shown that overexpressed spartin binds to the Ile44 hydrophobic pocket of ubiquitin, suggesting that spartin might have a ubiquitin-binding domain (UBD; Bakowska *et al.*, 2007).

Ubiquitination impacts a wide range of biological processes, including protein stability/degradation, DNA repair, endocytosis, autophagy, immunity, and inflammation (Husnjak and Dikic, 2012). Specificity of ubiquitin signaling is determined by the type of ubiquitin conjugation and by its interaction with different ubiquitin-binding proteins. Variation in ubiquitin conjugation results from the number of ubiquitin molecules added to a target protein, the type of linkage that forms ubiquitin chains (i.e., Lys-48 vs. Lys-63), and the dimension of the ubiquitin chain (i.e., linear vs. branched). Given

This article was published online ahead of print in MBoC in Press (<http://www.molbiolcell.org/cgi/doi/10.1091/mbc.E13-11-0705>) on February 12, 2014.

Address correspondence to: Joanna C. Bakowska (jbakowska@lumc.edu).

Abbreviations used: BMDC, bone marrow dendritic cells; DALIS, dendritic aggresome-like induced structures; DRIPS, defective ribosomal products; HSP, hereditary spastic paraplegias; HSQC, ¹H{¹⁵N}-heteronuclear single quantum coherence; LPS, lipopolysaccharide; TLR4, toll-like receptor four; UBD, ubiquitin-binding domain; UBR, ubiquitin-binding region.

© 2014 Karlsson *et al.* This article is distributed by The American Society for Cell Biology under license from the author(s). Two months after publication it is available to the public under an Attribution–Noncommercial–Share Alike 3.0 Unported Creative Commons License (<http://creativecommons.org/licenses/by-nc-sa/3.0>). "ASCB®," "The American Society for Cell Biology®," and "Molecular Biology of the Cell®" are registered trademarks of The American Society of Cell Biology.

the complexity of ubiquitin modification, it is not surprising that more than 20 different types of UBD families have been characterized (Husnjak and Dikic, 2012). These ubiquitin-binding proteins harbor UBDs that bind monoubiquitin and/or polyubiquitin chains. These families differ in both their protein structure and how their UBD interacts with ubiquitin.

Most UBDs are α -helical (Hicke *et al.*, 2005). Single or multiple α -helices are the secondary structures of UBDs, including the ubiquitin-associated domain of p62, the ubiquitin-interacting motif of ataxin-3, and the coupling of ubiquitin conjugation to endoplasmic reticular degradation domain of Vsp9 (Dikic *et al.*, 2009). However, nonhelical UBDs are categorized on the basis of similarities in functional domains. Unlike α -helical UBDs, which are found within secondary protein structures, these UBDs are located within loops resulting from tertiary folding of the protein. The pleckstrin homology folds of the proteasomal receptor Rpn13 uses loops rather than α -helices to bind ubiquitin, and this configuration allows the ubiquitin receptor to bind K48-linked di-ubiquitin and ubiquitin-like domains of ubiquitin-associated proteins (Husnjak *et al.*, 2008; Schreiner *et al.*, 2008). At the same time, the ubiquitin conjugating-like structures of the endosomal sorting complexes required for transport (ESCRT) trafficking protein Vps23/Tsg 101 interact with ubiquitin through two separate loop regions that enable it to sort ubiquitinated proteins into multivesicular bodies (Sundquist *et al.*, 2004; Teo *et al.*, 2004). The range of structural folds classified as UBDs is growing rapidly, and although most known UBDs contain defined secondary structures or distinct functional domains, it is likely that unique domains have yet to be discovered.

External stress, such as starvation, heat shock, or infection, can result in ubiquitination of misfolded proteins; these dysfunctional proteins, along with UBD-containing proteins, can form different types of aggregates within the cell cytoplasm. These aggregates are classified as aggresomes, aggresome-like induced structures, and dendritic aggresome-like induced structures (DALIS) based on their size, location, and cytoskeletal infrastructure. DALIS are large cytosolic structures that contain ubiquitinated proteins and are found in dendritic cells and macrophage cell lines upon maturation or after toll-like receptor four (TLR4) activation (Lelouard *et al.*, 2002; Canadien *et al.*, 2005). Unlike aggresomes, DALIS do not localize to the pericentriolar area, do not have a vimentin cage, and are not sensitive to microtubule or actin cytoskeletal disruptors (Lelouard *et al.*, 2004). DALIS are very transient; they are detected as soon as 4 h after TLR4 activation by lipopolysaccharide (LPS) and dissipate 20–44 h later (Lelouard *et al.*, 2002; Canadien *et al.*, 2005). DALIS contain defective ribosomal products (DRiPs) that, due to their errors in protein synthesis, are rapidly ubiquitinated and degraded (Yewdell *et al.*, 2001; Lelouard *et al.*, 2004; Pierre, 2005). It has been proposed that DRiPs are a primary source of endogenous antigenic peptides presented on MHC class 1 molecules and DALIS function as a holding ground for DRiPs, so DRiPs are processed and presented at a specific time for optimal T-cell activation (Pierre, 2005).

There is evidence that both proteasomal and autophagic proteins play a role in the formation of DALIS (Fujita *et al.*, 2011; Kettern *et al.*, 2011). Proteasomal chaperones, such as Bcl-2-associated athanogene 1 (BAG-1) and the E3 ubiquitin ligase, C terminus of Hsc70-interacting protein (CHIP), have been shown to colocalize with DALIS (Lelouard *et al.*, 2004; Kettern *et al.*, 2011). Overexpression of either BAG-1 or CHIP results in more DALIS; conversely, depletion of BAG-1 or CHIP decreases the number of DALIS in macrophages (Kettern *et al.*, 2011). Lack of BAG-1 or CHIP also results in defective antigen presentation in bone marrow dendritic cells (BMDCs), further supporting the role of DALIS, DRiPs, and protea-

somal degradation in antigen presentation and immune function (Kettern *et al.*, 2011). Both the autophagy receptor p62 and the autophagosome marker LC3 colocalize to DALIS (Fujita *et al.*, 2011; Kettern *et al.*, 2011). In particular, p62 has been shown to colocalize with LC3 at DALIS upon LPS stimulation of TLR4 and depletion of p62 decreases the occurrence of DALIS (Fujita *et al.*, 2011). These data suggest that both autophagy and proteasomal degradation play roles in DALIS regulation, antigen presentation, and immune function.

In this study we characterized the ubiquitin-binding properties of spartin. Building on evidence that spartin binds monoubiquitin, we investigated whether spartin binds ubiquitin chains, specifically, whether spartin binds to Lys-48 or Lys-63 chains. We used nuclear magnetic resonance (NMR) spectroscopy to characterize the ubiquitin-binding region (UBR) of spartin, and we defined the key amino acids in this region that are necessary for ubiquitin binding. Finally, we demonstrate a role for the UBR in DALIS formation.

RESULTS

Spartin localizes to DALIS and is important for the occurrence of DALIS

Previously we demonstrated that overexpressed spartin interacts with monoubiquitin and colocalizes with ubiquitin puncta in HeLa cells (Bakowska *et al.*, 2007). In the present study, we examined whether spartin localizes to specific structures, that is, DALIS, known to contain ubiquitinated proteins. DALIS have been shown to be repositories for ubiquitinated DRiPs, and several different proteins involved in autophagy and proteasomal degradation have been shown to localize to DALIS and to influence their occurrence (Lelouard *et al.*, 2004; Fujita *et al.*, 2011; Kettern *et al.*, 2011). We examined the distribution of endogenous spartin in the transformed murine macrophage cell line, RAW264.7, in which DALIS form after TLR4 activation (Canadien *et al.*, 2005). In untreated cells, spartin is mainly in the cytoplasm (Supplemental Figure S1A), but upon TLR activation via LPS treatment, endogenous spartin colocalized with both p62 and conjugated ubiquitin (Figure 1A, top). Importantly, overexpressed hemagglutinin (HA)-wild-type spartin also colocalized with p62 and conjugated ubiquitin in RAW264.7 cells treated with LPS (Figure 1A, bottom). We also investigated the expression of two major ubiquitin chains in DALIS. RAW264.7 cells treated with LPS for 12 h showed that endogenous spartin colocalized with p62 and Lys-63-linked ubiquitin and Lys-48-linked ubiquitin (Figure S1B). Endogenous spartin also colocalized with DALIS of LPS-treated BMDCs from wild-type C57BL/6J mice (Figure S2).

Protein levels of the autophagy receptor p62 and proteasomal chaperone BAG1 have been shown to increase upon LPS-induced formation of DALIS and decrease during DALIS degradation (Kettern *et al.*, 2011). Those findings suggest that both p62 and BAG1 have important functions in the processing of DALIS. However, although the protein levels of CHIP, an E3 ubiquitin ligase, do not change during LPS treatment, small interfering RNA knockdown of this ligase demonstrated that CHIP is necessary for DALIS formation and MHC class 1 antigen presentation (Kettern *et al.*, 2011). To examine spartin protein levels during DALIS formation, we immunoblotted the lysates from RAW264.7 cells treated with LPS for 0, 4, 8, 12, and 24 h and found that spartin protein levels did not change during DALIS formation or degradation (Figure S3).

Having established that spartin colocalizes with DALIS, we investigated whether depletion of spartin affects DALIS occurrence. To deplete spartin in RAW264.7 cells, we transduced the cells with spartin short hairpin RNA (shRNA) lentivirus particles. We used scrambled shRNA as a control. Immunoblots demonstrated that the

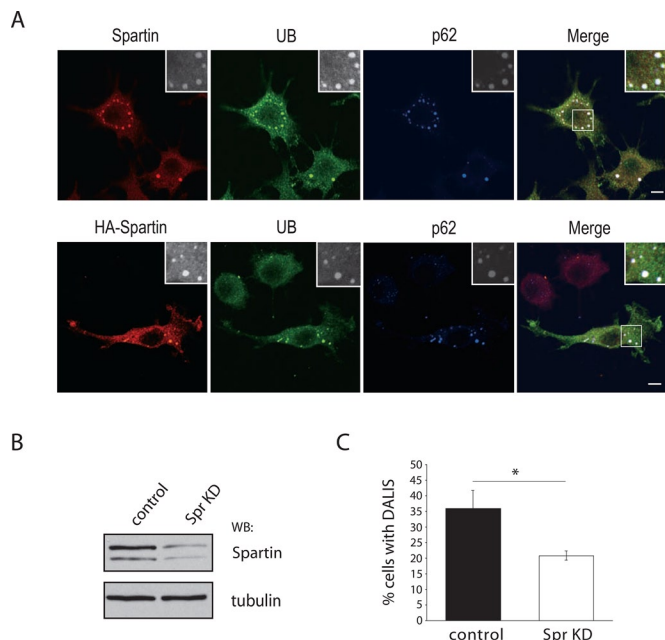


FIGURE 1: Spartin colocalizes with DALIS and is important for its formation. (A) Top, RAW264.7 cells treated with 10 ng/ml of LPS for 12 h were fixed and immunostained for endogenous spartin (red), conjugated ubiquitin (green), and p62 (blue). Bottom, RAW264.7 cells transfected with HA-spartin wild-type were treated with 10 ng/ml of LPS for 12 h; fixed; and immunostained for HA epitope (red), conjugated ubiquitin (green), and p62 (blue). Images are representative of at least three separate experiments. Scale bars: 5 μ m. (B) Lysates from RAW264.7 cells transfected with either scrambled shRNA (control) or spartin (SPG20) shRNA lentiviral vectors (Spr KD) were treated with 10 ng/ml of LPS for 12 h, harvested, resolved by SDS-PAGE, and immunoblotted using anti-spartin (top) or anti-tubulin (bottom) antibodies. (C) Quantification of DALIS in RAW264.7 cells transfected with control or SPG20 shRNA lentiviral vectors (Spr KD). Images were scored for the presence of DALIS, and the percentage of cells with DALIS was calculated by dividing the number of cells with DALIS by the total number of cells for each transduced cell pool. DALIS were defined as aggregates containing conjugated ubiquitin. Error bars represent mean \pm SEM from at least three independent experiments with more than 100 cells scored per experiment. *, $p < 0.05$.

spartin shRNA targets both isoforms of spartin (Figure 1B, top). Densitometric analysis of the immunoblots revealed that endogenous spartin protein levels were 70% lower in spartin-knockdown (KD) cells than in spartin-knockdown (KD) cells than in control shRNA-transduced cells. We also evaluated the effect of spartin KD on DALIS formation by examining the percentage of cells with DALIS in spartin-KD cells compared with control cells. Control and spartin-KD cells were treated with LPS for 12 h; fixed; and immunostained for spartin, conjugated ubiquitin, and p62. The number of spartin-KD cells that contained DALIS was significantly lower (~40%) than that of control cells (Figure 1C). This finding suggests that spartin has a role in the formation of DALIS and is consistent with the ability of spartin to bind ubiquitin and colocalize to ubiquitin puncta in vivo (Bakowska *et al.*, 2007).

Spartin binds directly to ubiquitin

We have shown in HeLa cells that overexpressed spartin (residues 208–408) can bind to ubiquitin (Bakowska *et al.*, 2007). In this study we performed in vitro binding experiments to determine whether the binding between spartin and ubiquitin is direct. We used dele-

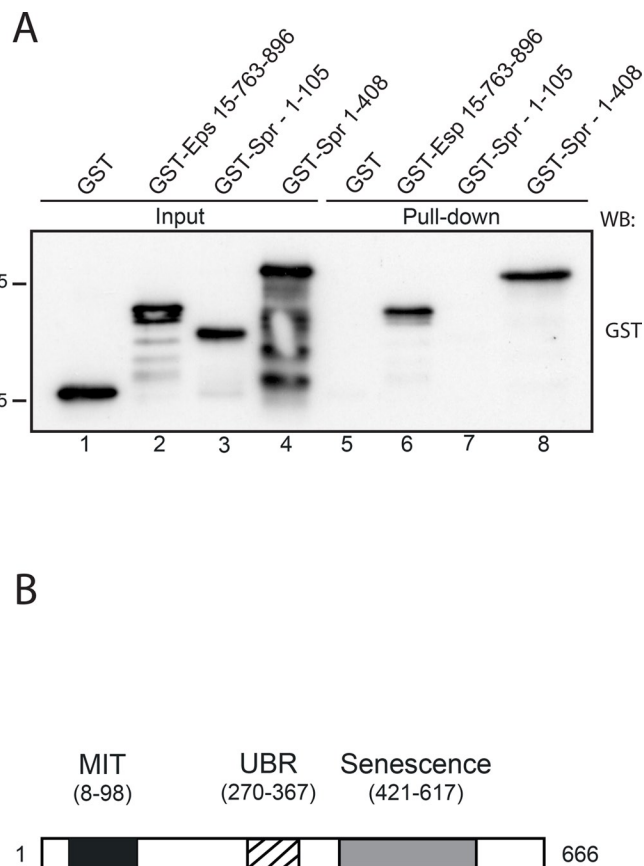


FIGURE 2: Spartin directly binds to monoubiquitin. (A) GST, GST-Eps15-763-896, GST Spr1-105, or GST-Spr 1-408 proteins were eluted from glutathione beads and incubated with ubiquitin agarose. Ubiquitin agarose was washed, and bound proteins were eluted with Laemmli buffer and resolved by SDS-PAGE. Immunoblotting was performed with anti-GST antibody. (B) Schematic diagram of full-length spartin, showing the MIT domain, plant-related senescence domain, and a UBR. Numbers represent the amino acid residues of the indicated domain.

tion constructs of glutathione S-transferase (GST)-spartin (eluted from the beads) and ubiquitin bound to agarose beads. We found that spartin (amino acids 1–408) and the ubiquitin-interacting motif (UIM) of Eps15 (763–896), which was used as a positive control, both bound to ubiquitin linked to beads (Figure 2A). In contrast, neither spartin 1–105, which contains the MIT domain, nor GST alone bound to ubiquitin. We made several other deletion constructs of spartin and performed in vitro binding assays with Lys-63-linked ubiquitin (Figure S4)

We found that GST-spartin 186–340 bound to ubiquitin, but GST-spartin 186–330 did not, suggesting that the amino acids important for binding to ubiquitin are within the region 330–340 (Figure S4, A and C). Additional results revealed that the GST-spartin 108–408 bound to ubiquitin, but GST-spartin 108–250 and 295–408 did not (Figure S4, B and C). These data indicate that the 250–295 and 330–340 regions of spartin are necessary but not sufficient for binding to ubiquitin. Overall both of these regions of spartin have to be present in order to bind ubiquitin.

Taken together (Figures 2A and S4), our results suggest that two subregions within amino acids 250–340 are necessary for the binding of spartin to ubiquitin, as removal of either the 250–295 or the 330–340 region results in no binding of spartin to ubiquitin. We named

this new UBD, ranging from amino acids 250 to 340, the ubiquitin-binding region (UBR; shown in Figure 2B). The UBR alone did not express well in bacteria; therefore all subsequent experiments were performed using amino acid residues 155–367 of spartin.

The spartin UBR consists of two segments

We used NMR spectroscopy to determine how spartin's UBR binds to ubiquitin. Because chemical shifts in backbone amide protons and nitrogens are exquisitely sensitive to changes in the chemical environment induced by protein complexity, they can be used to identify protein–protein interaction surfaces (Zuiderweg, 2002). The spartin UBR was titrated into [U - ^{15}N]ubiquitin, and chemical-shift changes were monitored by $^1H\{^{15}N\}$ -heteronuclear single quantum coherence (HSQC) NMR (Cavanagh *et al.*, 2007). As we increased the concentration of spartin UBR, we observed the gradual disappearance of a set of ubiquitin peaks (Figures 3A and S5). There were only minor (<0.04 ppm) changes in the positions of the ubiquitin peaks. These changes are indicative of chemical exchange between free ubiquitin and spartin UBR-bound [U - ^{15}N]ubiquitin on the intermediate NMR timescale. These data suggest that the binding affinity of the spartin UBR for ubiquitin is below $10 \mu M$ (Matsuo *et al.*, 1999; Xie *et al.*, 2007). This binding affinity is much stronger than the binding affinities of well-characterized ubiquitin-interacting motif peptides for ubiquitin, which are mostly above $100 \mu M$ (Shekhtman and Cowburn, 2002; Polo *et al.*, 2003; Hirano *et al.*, 2006).

Mapping residues affected by spartin UBR onto ubiquitin structure revealed a contiguous interaction surface that consists of a classical ubiquitin interaction surface (Shekhtman *et al.*, 2002) formed by Leu-8, Ile-44, Ala-46, Gly-47, Lys-48, Gln-49, His-68, Val-70, Leu-71, Arg-72, and Leu-73, as well as an extended surface patch formed by Leu-6, Thr-7, Thr-9, Gly-10, Lys-11, and Thr-12 (Figures 3B and S5). This patch is located in the immediate vicinity of the ubiquitin-binding surface and may explain the tighter binding of the spartin UBR to ubiquitin compared with the UBDs of other proteins (Buz and Shekhtman, 2008). The HSQC spectrum of free [U - ^{15}N]spartin UBR revealed backbone amide proton and nitrogen peaks between 7.5 and 8.5 ppm (Figure 4A). Some peaks in this spectral region also exhibited significant broadening, which is indicative of the lack of spartin UBR structure. Based on the assigned chemical shifts (Wishart and Sykes, 1994), the spartin UBR does not contain any α -helical segments and is most likely formed from tertiary folds or loops. The lack of α -helical structure in UBDs is a common feature of adaptor proteins (Pietrosemoli *et al.*, 2013).

To determine the binding epitope of the spartin UBR on ubiquitin, we increased the concentration of ubiquitin and monitored changes in [U - ^{15}N]spartin UBR HSQC spectra (Figure 4A). Again, we observed broadening of the subset of spartin UBR peaks. Spartin UBR residues affected by ubiquitin binding, namely, residues 160–165, 273–275, 330–332, and 360–363, were located in four different regions of the primary structure (Figure 4B and C). We mutated the amino acids in each of these regions to alanines in order to determine which regions contribute most of the ubiquitin-binding energy. Mutation of DWL 273–275 (Figure S6A) or MSD 330–332 (Figure S6B) to alanine weakened the binding of the spartin UBR to ubiquitin above $200 \mu M$. It is likely that these two segments bind to ubiquitin such that mutating one segment is sufficient to disrupt the spartin UBR–ubiquitin interaction.

Mutational analysis of the UBR of spartin

The spartin UBR, spanning amino acids 250–340, showed significant broadening when bound with ubiquitin. Within this region, the amino acids DWL 273–275 and MSD 330–332 are conserved among

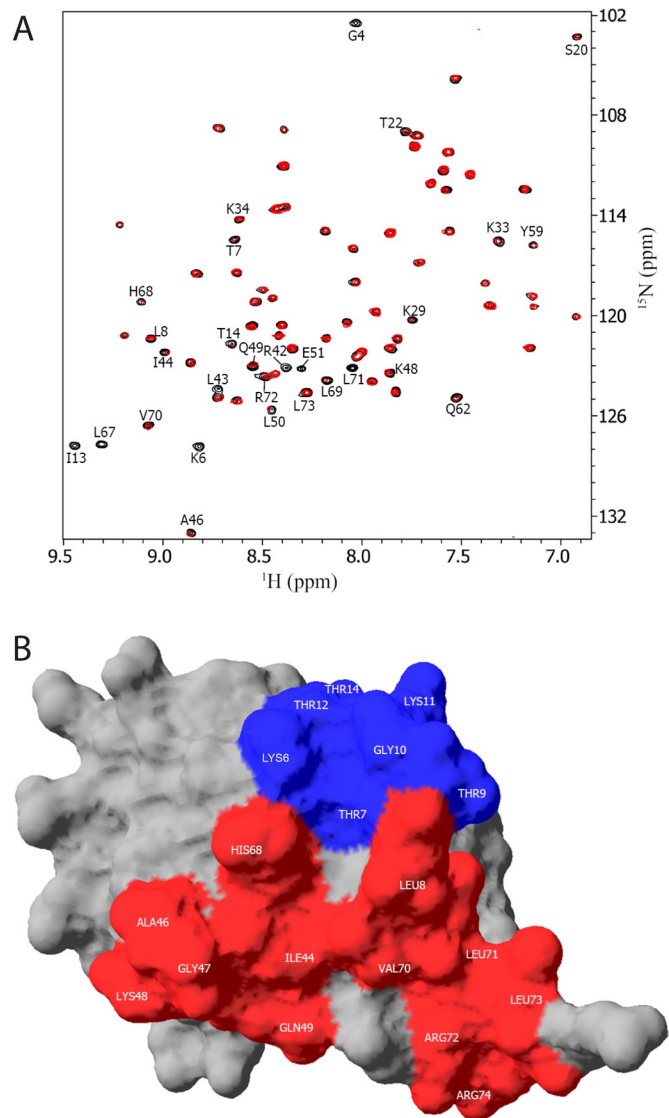


FIGURE 3: The ubiquitin–spartin interaction surface consists of a classical interaction surface and an extended surface patch. (A) Overlay of HSQC spectra showing free $2.5 \mu M$ [U - ^{15}N]ubiquitin (black) and the $2.5 \mu M$ [U - ^{15}N]ubiquitin–spartin 155–367 complex (red) with molar ratio 1:10. Due to ^{15}N editing, only backbone amide protons and nitrogens of ubiquitin are present in the spectrum. Most peaks do not change their positions. A subset of ubiquitin peaks that are substantially broadened due to ubiquitin interaction with spartin 155–367 is labeled. (B) Residues of ubiquitin that underwent significant broadening (more than 40%) during the NMR titration experiment are shown in red and blue. Ubiquitin residues involved in binding to a classical ubiquitin interaction surface are shown in red. The extended ubiquitin–spartin interacting surface is shown in blue.

various species. To further understand how spartin binds to ubiquitin, we mutated DWL 273–275 and/or MSD 330–332 to alanines and generated three different mutation constructs: spartin GST–spartin 155–367 (mutant I), GST–spartin 155–367 (mutant II), and GST–spartin 155–367 (mutant III, described in *Materials and Methods*). These mutants and wild-type spartin 155–367 (GST–spartin 155–367 WT) were used in a series of *in vitro* binding experiments to determine how spartin interacts with ubiquitin.

We incubated wild-type spartin 155–367 and spartin 155–367 mutants I, II, or III with GST–di-ubiquitin (2xUB) or GST–tetra-ubiquitin

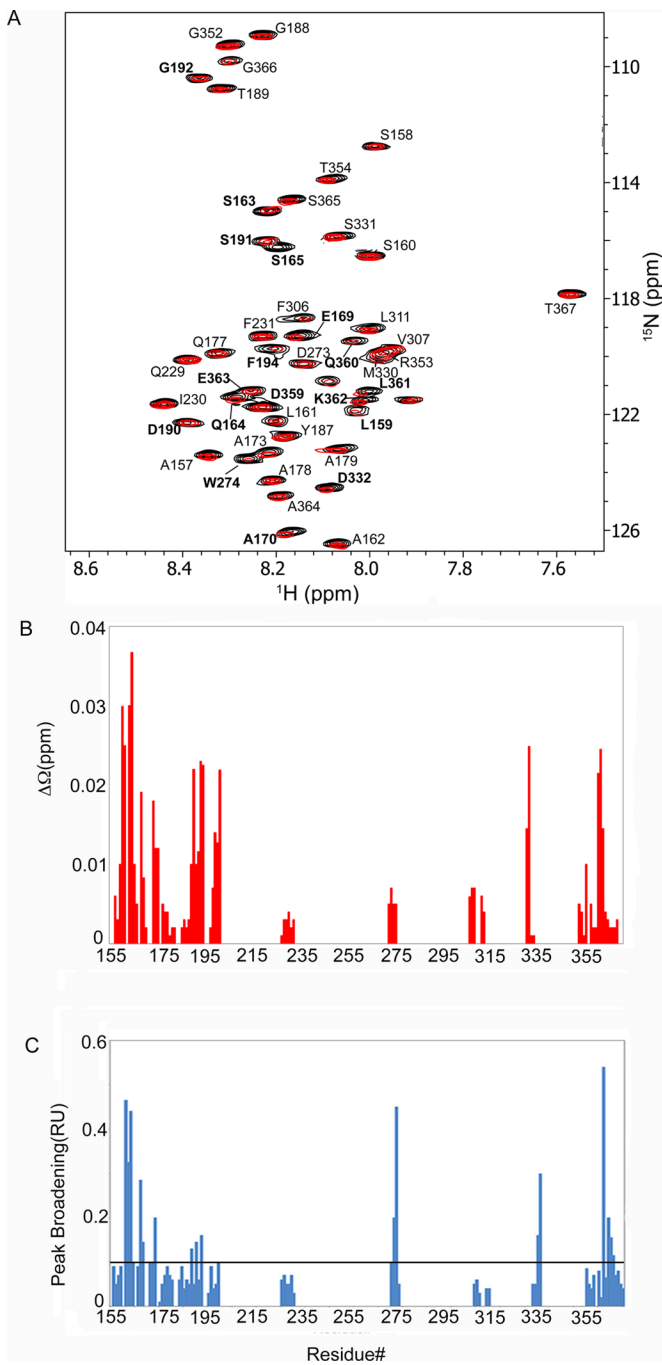


FIGURE 4: Spartin's interaction surface with ubiquitin consists of two main segments. (A) An overlay of HSQC spectra showing free 5 μM [$U\text{-}^{15}\text{N}$]spartin 155-367 (black) and the 5 μM [$U\text{-}^{15}\text{N}$]spartin 155-367-ubiquitin complex with molar ratio 1:10 (red). Due to ^{15}N editing, only backbone amide protons and nitrogens of spartin 155-367 are present in the spectrum. Most peaks do not change their positions, as only a subset of spartin 155-367 residues interact with ubiquitin. Spartin 155-367 peaks that have broadened substantially or completely are labeled. (B) Amide chemical shift difference for all the assigned residues in free and ubiquitin-bound spartin 155-367. Calculations are described in the *Materials and Methods*. (C) Peak broadening for all the assigned residues in free and ubiquitin-bound spartin 155-367. Peak broadening above 10% is considered to be significant. Calculations are described in *Materials and Methods*.

(4xUB). Bound proteins were resolved by SDS-PAGE and immunoblotted to detect which spartin proteins bound to ubiquitin. As shown in Figure 5A, spartin 155-367 WT interacted with both 2xUB and 4xUB. However, none of the three mutant spartin proteins was able to bind any of the ubiquitin chains.

We also examined the interaction of the UBR of spartin in the context of full-length WT and full-length mutant III spartin proteins expressed in HeLa cells to 1xUB, 2xUB, and 4xUB (Figure 5B). Using a luminescence-based mammalian interactome (LUMIER) assay, we found that the full-length WT spartin showed the strongest binding to 2xUB, followed by binding to 1xUB (Figure 5B). WT spartin's ability to bind 4xUB was four times weaker than its binding to 2xUB. As expected, spartin mutant III did not bind to any species of ubiquitin (Figure 5B).

Finally, we tested the capacity of GST-spartin 155-367 and the spartin mutants I, II, or III to bind polyubiquitin Lys-63-linked ubiquitin chains. As shown in Figure 5C, GST-spartin 155-367 and GST-p62 (used as a positive control) bound to Lys-63-linked ubiquitin chains, but none of the GST-spartin mutants bound to Lys-63-linked ubiquitin chains. In contrast, GST-spartin 155-367 did not show binding to Lys-48-linked ubiquitin chains (Figure 5D) compared with the positive control, 19S proteasomal subunit, Rpn10/S5a, which did interact with Lys-48-linked chains.

Spartin's UBR is important for the occurrence of DALIS

Having established a role for spartin in DALIS formation and defined the UBR of spartin, we determined whether this region was necessary for spartin's role in the formation of DALIS. RAW264.7 cells were transfected with either empty HA vector (control), HA-tagged wild-type spartin (Spr-WT), or HA-tagged spartin containing mutations of DWL 273-275 and MSD 330-332 to alanine (Spr-mut III). After transfection, the cells were treated with LPS, fixed, and examined for DALIS by using immunofluorescence (Figure 6A). As expected, cells transfected with HA-tagged vector did not colocalize with either conjugated ubiquitin or p62 (Figure 6A, top row). Wild-type spartin colocalized with both p62 and ubiquitin (Figure 6A, second row) in a manner similar to that of BAG-1 (Figure 6A, fourth row). However, overexpressed spartin mutant III did not colocalize with either p62 or ubiquitin in DALIS (Figure 6A, third row).

Overexpression of spartin led to a significant increase (~26% more) in the number of cells with DALIS ($63 \pm 7\%$) compared with control cells transfected with an empty vector ($50 \pm 2\%$) and caused a greater increase in the number of cells with DALIS compared with our positive controls, BAG-1 (~53%; Figure 6B) and CHIP (~57%; data not shown). Although cells transfected with mutant spartin showed less (~10% less) DALIS formation, there was no significant difference in the percentage of cells with DALIS in cells transfected with the spartin mutant III ($45 \pm 8\%$) compared with cells transfected with control vector ($50 \pm 2\%$) (Figure 6B). We also examined DALIS formation in cells expressing spartin mutant II and unlike cells expressing spartin mutant III, there was no decrease in DALIS formation compared with control cells (~50%; unpublished data). The percentage of cells in which spartin colocalized with DALIS was significantly different between cells transfected with mutant spartin ($33 \pm 7\%$) and cells transfected with wild-type spartin ($76 \pm 8\%$) (Figure 6C). These findings suggest that spartin's colocalization with DALIS depends on spartin's ability to bind to ubiquitin.

Next we examined whether the decreased occurrence of DALIS in spartin-KD cells could be rescued by overexpression of human spartin. We chose to use human spartin, because the RNA is not

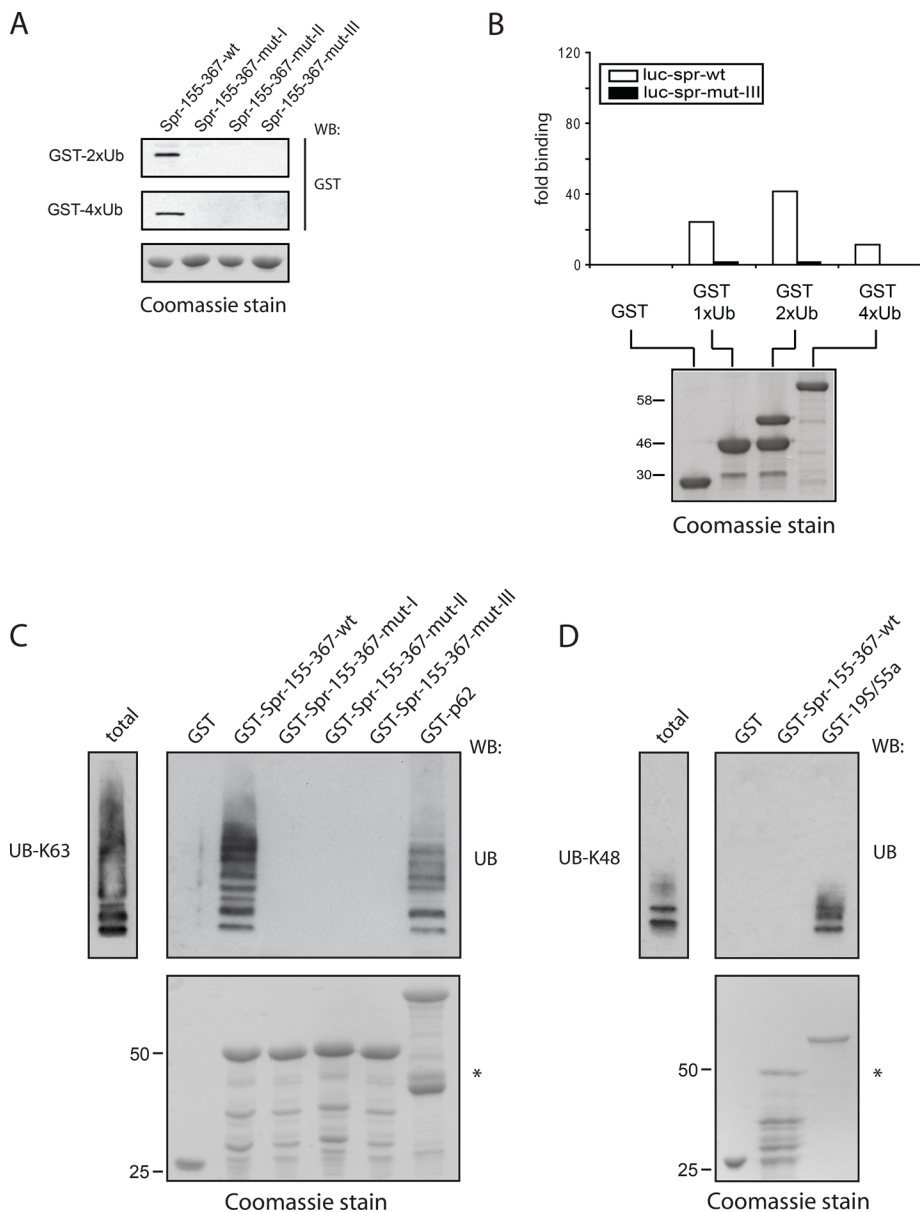


FIGURE 5: Spartin UBR binds different species of ubiquitin. (A) Indicated spartin proteins were digested with PreScission to remove the GST tag and then incubated with GST-2xUB or GST-4xUB. After washes, the bound proteins were eluted with Laemmli buffer, resolved by SDS-PAGE, and immunoblotted with anti-ubiquitin antibody. Spartin proteins used for this experiment were resolved by SDS-PAGE and stained with Coomassie (bottom). (B) Purified ubiquitin (1xUB), di-ubiquitin (2xUB), and tetra-ubiquitin (4xUB) GST-fusion proteins or GST alone were incubated with lysates of HeLa cells expressing luciferase spartin and processed as described in *Materials and Methods*. The fold increase of luciferase activity bound to beads over negative control (GST alone) is shown. Bottom, GST-fusion protein stained with Coomassie. (C) Indicated GST-spartin proteins, GST-p62, or GST alone were incubated with Lys-63-linked ubiquitin chains (UB-K63). After incubation and washes, the bound proteins were eluted with Laemmli buffer, resolved by SDS-PAGE, and immunoblotted with anti-ubiquitin antibody. Coomassie-stained gel (bottom) shows that similar amounts of fusion proteins were used for the pull-down experiments. (D) Indicated GST-spartin proteins, GST-195/55a protein, or GST alone were incubated with Lys-48-linked ubiquitin chains (UB-K48). After incubation and washes, the bound proteins were eluted with Laemmli buffer, resolved by SDS-PAGE, and immunoblotted with anti-ubiquitin antibody. Coomassie-stained gel (bottom) shows that similar amounts of fusion proteins were used for the pull-down experiments.

completely homologous to murine spartin RNA; therefore it would not be targeted by our murine shRNA lentivirus. Indeed, the lysates from spartin-KD cells transfected with either HA-tagged wild-type

UBD but did not determine the specific amino acids critical for this interaction (Bakowska *et al.*, 2007). In the present studies, to characterize the UBR of spartin, we used NMR to examine the interaction

human spartin or HA-tagged mutant human spartin (Spr-mut III) showed equal expression of both constructs (Figure 7A). Spartin-KD cells expressing empty HA vector, HA-tagged wild-type human spartin, or HA-tagged mutant human spartin were treated with LPS, fixed, and immunostained to evaluate how these proteins affect the formation of DALIS. Overexpression of wild-type human spartin rescued the DALIS phenotype in spartin-KD cells. Cells rescued with wild-type human spartin ($40 \pm 0.6\%$) had significantly more (~20% more) DALIS than control cells ($32 \pm 1.2\%$) (Figure 7B). In contrast, the spartin mutant did not significantly increase the percentage of cells that contained DALIS ($33 \pm 2.2\%$), suggesting that it does not rescue the spartin-KD phenotype. These findings support the hypothesis that the formation of DALIS depends on spartin's ability to bind ubiquitin.

DISCUSSION

In this study, we showed that spartin plays a functional role in the formation of DALIS. After LPS stimulation of TLR4, spartin colocalized with DALIS in both RAW264.7 cells and primary mouse BMDCs. Depletion of spartin resulted in decreased formation of DALIS. Conversely, overexpression of wild-type spartin increased the number of cells with DALIS in the parental cell line and rescued the depleted DALIS in spartin-KD cells. This effect on the formation of DALIS depends on spartin's ability to bind ubiquitin. Spartin mutants, in which the residues DWL 273–275 and MSD 330–332 were mutated to alanine, did not colocalize with DALIS. Compared with overexpressed wild-type spartin, these mutants did not significantly increase the number of cells with DALIS. Furthermore, these mutants were unable to rescue the attenuated DALIS formation after spartin knockdown.

We also observed colocalization of spartin with proteins involved in the regulation of DALIS. Both endogenous and overexpressed spartin colocalized with p62 in DALIS. Spartin has also been shown to interact with p62 (Urbanczyk and Enz, 2011), which is an autophagy receptor necessary for DALIS formation (Fujita *et al.*, 2011). TLR4 signaling through MyD88 and p38 mitogen-activated protein kinase increases p62 mRNA and protein (Fujita *et al.*, 2011). Knockdown of p62 decreased DALIS formation, as did knockdown of spartin.

Our previous work with overexpressed spartin suggested that spartin contains a

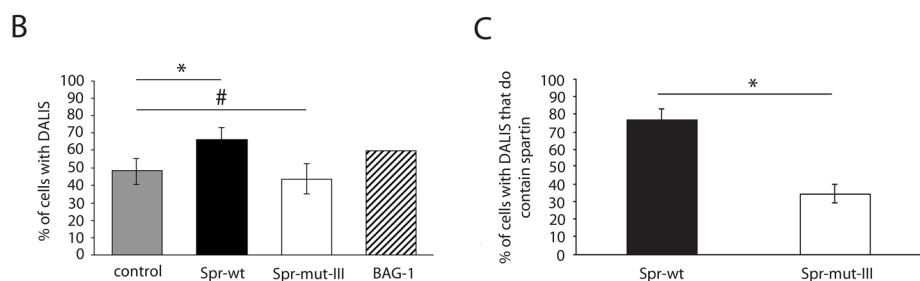
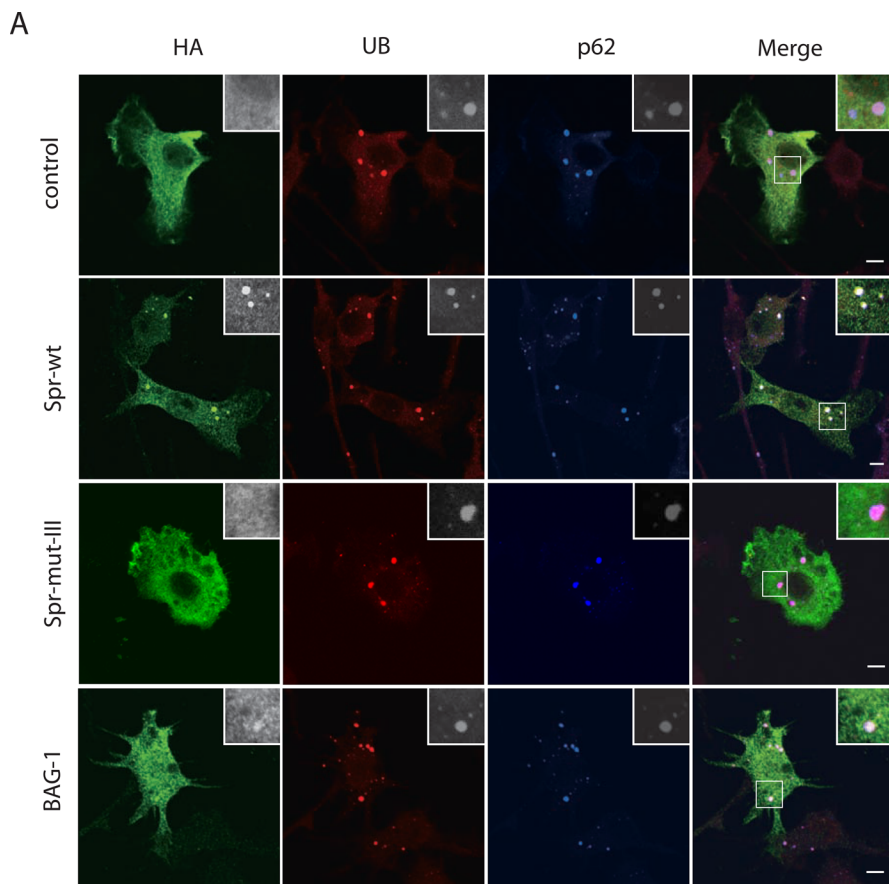


FIGURE 6: The UBR of spartin is important for its localization to DALIS and for the formation of DALIS. (A) RAW264.7 cells were transfected with HA-empty vector (control, top row), HA-spartin wild-type (Spr-WT, second row), HA-spartin mutant III (Spr-mut-III, third row), or HA-BAG1 (BAG-1, fourth row), and treated with 10 ng/ml of LPS for 12 h. Cells were fixed and immunostained for HA epitope (green), conjugated ubiquitin (red), and p62 (blue). Images are representative of at least three separate experiments. Scale bars: 5 μ m. (B) Quantification of DALIS in RAW264.7 cells transfected with the indicated vectors. DALIS were defined as aggregates containing conjugated ubiquitin. Images were scored for the presence of DALIS, and the percentage of cells with DALIS was calculated by dividing the number of cells with DALIS by the total number of cells transfected for each construct. Error bars represent mean \pm SEM from at least three independent experiments with more than 50 cells scored per experiment. *, $p < 0.05$; #, $p > 0.05$. (C) Quantification of DALIS that contain spartin in RAW264.7 cells transfected with HA-spartin wild-type or HA-spartin mutant III. Images were scored for the presence of DALIS and spartin. DALIS were defined as aggregates containing conjugated ubiquitin. Percentage of cells with DALIS and spartin was calculated by dividing the number of cells with DALIS and spartin by the total number of cells transfected for each construct. Error bars represent mean \pm SEM from at least three independent experiments with more than 50 cells scored per experiment. *, $p < 0.001$.

of spartin and monoubiquitin. We mapped residues affected by the spartin UBR onto ubiquitin and found two separate areas of ubiquitin affected by spartin binding. The first interaction surface con-

sists of a classical ubiquitin interaction surface formed by Leu-8, Ile-44, Ala-46, Gly-47, Lys-48, Gln-49, His-68, Val-70, Leu-71, Arg-72, and Leu-73 (Shekhtman and Cowburn, 2002). This classical ubiquitin interaction surface is also found in UIM domains (Shekhtman *et al.*, 2002). The spartin UBR also interacts with ubiquitin at a second extended surface patch formed by Leu-6, Thr-7, Thr-9, Gly-10, Lys-11, and Thr-12. This interaction surface might be responsible for the higher binding affinity of spartin for ubiquitin compared with other UBDs. These data confirm our previous biochemical findings that spartin interacts with ubiquitin via its Ile-44 hydrophobic pocket; they also demonstrate that the spartin UBR consists of both classical and unique ubiquitin-binding surfaces (Bakowska *et al.*, 2007).

The NMR spectra of spartin interacting with ubiquitin also revealed two segments of spartin involved in spartin-ubiquitin interactions: DWL 273–275 and MSD 330–332. Mutation of these amino acid regions to alanines indicated that DWL 273–275 and MSD 330–332 were both necessary for the spartin-ubiquitin interaction. Using GST pull-down assays, we confirmed that these two conserved domains were also necessary for spartin's binding to Lys-63-linked polyubiquitin chains. Lys63-linked ubiquitination has been shown to play a role in cell signaling, trafficking, DNA damage, and immunity, whereas Lys-48-linked ubiquitination is a well-known proteasomal degradation signal (Husnjak and Dikic, 2012). The fact that spartin interacts only with Lys-63-linked ubiquitin suggests that it is likely to be involved in cell signaling, trafficking, and/or repair. Future studies are planned to examine the role of spartin in each of those cellular processes.

Our NMR data for unbound spartin suggest that spartin does not have a definitive tertiary structure. This lack of tertiary structure suggests that the UBR of spartin is not a classical α -helical UBD. It is more likely to resemble the UBDs of Rpn13 and Vps23/Tsg101, which consist of loops formed from tertiary structure folds.

Troyer syndrome is a complex HSP caused by a frameshift mutation in the spartin gene (Patel *et al.*, 2002). No spartin protein is detected in the tissue of affected individuals, and this lack of protein results in loss-of-function pathophysiology (Bakowska *et al.*, 2008; Manzini *et al.*, 2010). Degradation of the corticospinal motor neurons results in progressive lower limb spasticity and

weakness, which occurs in patients with either pure or complicated HSPs. Patients with complicated HSPs also present with additional symptoms, such as cognitive impairment, distal amyotrophy,

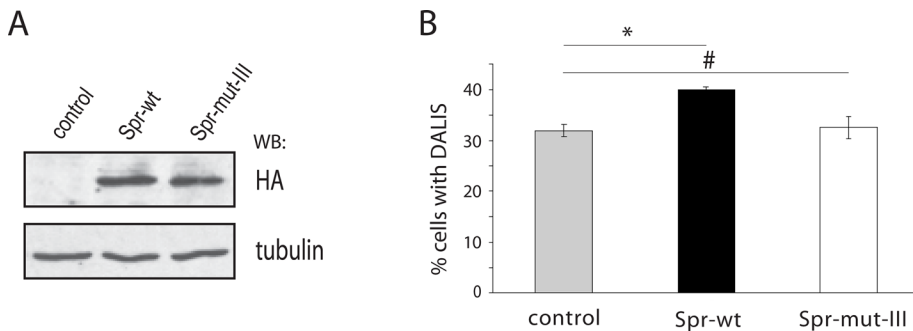


FIGURE 7: UBR of spartin is important for the formation of DALIS. (A) RAW264.7 cells transduced with spartin shRNA lentivirus (SPG20 KD) were transfected with HA-empty vector (control, lane 1), HA-spartin wild-type (Spr-wt, lane 2), or HA-spartin mutant III (Spr-mut-III, lane 3). Lysates from transfected SPG20-KD cells were harvested, resolved by SDS-PAGE, and immunoblotted with anti-HA epitope (top) or anti-tubulin antibodies (bottom). (B) Quantification of DALIS in RAW264.7 cells. Cells transduced with spartin shRNA lentivirus (SPG20 KD) were transfected with HA-empty vector (control), HA-spartin wild-type (Spr-wt), or HA-spartin mutant III (Spr-mut-III). After treatment with 10 ng/ml of LPS for 12 h, cells were processed for immunofluorescence. Images were scored for the presence of DALIS, and the percentage of cells with DALIS was calculated by dividing the number of cells with DALIS by the total number of cells transfected for each representative construct. DALIS were defined as aggregates containing conjugated ubiquitin. Error bars represent mean \pm SEM from three independent experiments with more than 50 cells scored per experiment. *, $p < 0.05$; #, $p > 0.05$.

retinopathy, ataxia, thin corpus callosum, and peripheral neuropathy, which most likely result from degeneration of axons in the brain. Neurodegeneration is also a hallmark of several other types of neurological diseases, such as Alzheimer's disease (AD) and amyotrophic lateral sclerosis (ALS; Amor *et al.*, 2010). A common feature of these diseases is immune activation in the CNS, and chronic neuroinflammation is thought to contribute to the progression of neuronal damage in those diseases (Amor *et al.*, 2010). In particular, TLR4 signaling has been linked to AD and ALS (Lehnhardt, 2010; Okun *et al.*, 2011). TLR4 is activated in brain cells of individuals with AD. In microglia, TLR4 stimulus attenuates AD by enhancing clearance of β -amyloid, whereas in neurons, it exacerbates the disease by increasing neuronal vulnerability to oxidative stress and β -amyloid toxicity (Okun *et al.*, 2011). ALS is characterized by degeneration of motor neurons. When exposed to activation of TLR4 signaling via systematic LPS administration, mice expressing the ALS linked superoxide dismutase 1 mutation (SOD1^{G37R}) had accelerated disease progression and motor axon degeneration (Nguyen *et al.*, 2004). At present, we can only speculate how the immune system and TLR4 signaling contribute to HSPs, but our previous work with epidermal growth factor receptor (EGFR) suggests that spartin plays a role in TLR4 trafficking. We showed that spartin knockdown in HeLa cells decreases the rate of EGFR internalization and degradation (Bakowska *et al.*, 2007). TLR4 receptor signaling, like EGFR, is also down-regulated via clathrin-mediated endocytosis then sorted to late endosomes for subsequent degradation by lysosomes (Husebye *et al.*, 2006). Spartin might affect the signaling transduction of TLR4 in a manner similar to that of EGFR, and future studies will focus on how spartin contributes to TLR4 endocytosis, endosomal sorting, and signaling. In the absence of spartin, TLR4 would not be degraded, and TLR4 signaling would be greater. Like AD or ALS, this could result in immune dysfunction, which in turn could contribute to the neurodegenerative effects seen in Troyer syndrome.

In summary, we have demonstrated spartin's role in the formation of DALIS, which depends on spartin's ability to bind Lys-63-linked ubiquitin chains via the conserved amino acid residues DWL 273–275 and MSD 330–332. These conserved domains are

necessary for the strong interaction between the spartin UBR and ubiquitin. This interaction is formed by the binding of the nonhelical spartin UBR to both classical and unique amino acid sequences in ubiquitin. Future studies will investigate whether the effect of spartin on DALIS formation is due to the involvement of spartin in TLR4 signaling, proteasomal degradation, or autophagy.

MATERIALS AND METHODS

Antibodies and reagents

The following primary antibodies were obtained commercially: rabbit anti-spartin (13791-1-AP; Proteintech, Chicago, IL), guinea pig anti-p62 (GP62-C; Progen, Heidelberg, Germany), mouse anti-monoubiquitin and polyubiquitin conjugates, clone FK2 (BML-PW8810; Enzo Life Sciences, Farmingdale, NY), rabbit anti-BAG1 (sc-939-G; Santa Cruz Biotechnology, Santa Cruz, CA), rabbit anti-HA tag (ab9110; Abcam, Cambridge, MA), mouse anti- β -actin (clone AC-74; Sigma-Aldrich, St. Louis, MO), mouse anti- β -tubulin (E7; Developmental Studies Hybridoma Bank, University of Iowa, Iowa City, IA), mouse anti-polyubiquitin (K⁶³-linkage-specific), mAb (HWA4C4) (BML-PW0600; Enzo Life Sciences), mouse Milli-Mark anti-ubiquitin, Lys-48-Specific-FITC, clone Apu2 (FCMAB294F; Millipore, Billerica, MA), anti-CHIP rabbit antibody (PC711; Millipore), and anti-mouse ubiquitin mouse anti-ubiquitin (P41D; Covance, Princeton, NJ). The following secondary antibodies used for immunoblotting were obtained from Thermo Fisher Scientific (Lafayette, CO): goat anti-rabbit immunoglobulin G (IgG) horse-radish peroxidase (HRP) (#31460), goat anti-mouse IgG HRP (#31430), and rabbit anti-goat IgG HRP (#31420). The secondary goat anti-guinea pig IgG HRP (sc-2438) was purchased from Santa Cruz Biotechnology. The following secondary antibodies used for immunofluorescence were obtained from Invitrogen (Carlsbad, CA): Alexa Fluor 568 (goat anti-rabbit IgG [A11036]) and goat anti-mouse IgG [A11031], Alexa Fluor 488 (goat anti-rabbit IgG [A11034]) and goat anti-mouse IgG [A11029], and Alexa Fluor 633 goat anti-guinea pig IgG (A21105).

Reagents were purchased as follows: lipopolysaccharide (LPS), 2-mercaptoethanol, and puromycin from Sigma-Aldrich; pGEX-6P-1 vector and PreScission protease from GE Healthcare Life Sciences (Waukesha, WI); lipofectamine, GlutaMAX, and ProLong Gold Antifade Reagent from Invitrogen; DMEM/F12, sodium pyruvate and nonessential amino acids from HyClone (Lafayette, CO); fetal bovine serum (FBS) from Gemini Bio-Products (West Sacramento, CA); cell culture plates from Sarstedt (Nümbrecht, Germany); polybrene, Immobilon-P membrane, and Luminata Forte ECL reagent from Millipore; protease inhibitor cocktail from Roche (Indianapolis, IN); nitrocellulose (0.45 μ m) from Thermo Scientific; RapidBlock solution from Amresco (Framingham, MA); gradient gels (4–20%) from Bio-Rad (Hercules, CA); nylon mesh (9072520) from BD Falcon (Franklin Lakes, NJ); and murine granulocyte macrophage colony-stimulating factor (GM-CSF) from Peprotech (Rocky Hill, NJ; #315-03).

Mammalian and bacterial expression plasmids

A fragment of spartin cDNA (residues 155–367) was cloned into the XhoI and EcoRI site of the pGEX-6P-1 vector, and this plasmid was

named pGEX-WT Spr 155-367. Generation of pGEX-spartin 155-367 (DWL 273-275AAA) mutant I was accomplished by site-directed mutagenesis of aspartic acid, tryptophan, and leucine (Asp-273, Trp-274, Leu-275) residues within spartin to alanine in plasmid pGEX-6P-1-WT spartin 155-367 WT. For generation of pGEX-spartin 155-367 (MSD 330-332AAA) mutant II, site-directed mutagenesis of methionine, serine, and aspartic acid (Met-330, Ser-331, Asp-332) residues to alanine was accomplished in plasmid pGEX-6P-1-WT spartin 155-367. pGEX-spartin 155-367-mutant (DWL 273-275AAA; MSD 330-332AAA), mutant III, was generated by site-directed mutagenesis of aspartic acid, tryptophan, and leucine (Asp-273, Trp-274, Leu-275) residues and methionine, serine, and aspartic acid (Met-330, Ser-331, Asp-332) residues to alanine in plasmid pGEX-6P-1-WT spartin 155-367. All mutations were performed using the QuikChange protocol according to the manufacturer's instructions.

NMR studies

Human ubiquitin was expressed by using pet3aUbq (Burz *et al.*, 2006). The following plasmids were used to express the predicted UBR of human WT and mutant spartin in bacteria: pGEX6p-1-WT spartin 155-367, pGEX6p-1-spartin 155-367 (273-275AAA), mutant I, and pGEX6p-1-spartin 155-367 (330-332AAA), mutant II. For U - ^{15}N labeling, cells were grown at 37°C in minimal medium (M9) containing 100 mg/l ampicillin and 1 g/l [^{15}N]ammonium chloride as the sole nitrogen source. For U - ^{13}C , ^{15}N labeling, cells were grown at 37°C in M9 medium containing 100 mg/l ampicillin, 1 g/l [^{15}N]ammonium chloride, and 2 g/l [^{13}C]glucose instead of unlabeled glucose as the sole carbon source. Proteins were purified as described previously (Hooper *et al.*, 2010). We applied PreScission protease to remove the N-terminal GST tag from GST-WT spartin 155-367, and GST-spartin 155-367 (273-275AAA), mutant I; and GST-spartin 155-367 (330-332AAA), mutant II. All proteins were dialyzed into 10 mM potassium phosphate (pH 7.0), 100 mM NaCl.

Colocalization studies in RAW264.7 cells

For overexpression studies, RAW264.7 cells were transfected with mammalian expression vectors using Lipofectamine. The mammalian expression vector pGW1-HA-spartin was described previously (Bakowska *et al.*, 2007), and the same mutations as in the pGEX-6P-1-spartin vector were used to generate pGW1-HA-spartin mutants I, II, and III. We received the pDNA wild-type BAG1-HA vector from R. Morimoto (Northwestern University; Song *et al.*, 2001).

Cell culture

RAW264.7 cells were used from passages 7–15 and maintained in DMEM/F12 supplemented with 10% FBS, nonessential amino acids, and GlutaMAX. To induce DALIS formation, we treated cells with 10 ng/ml of LPS for 12 h.

BMDC protocol

BMDCs were harvested and cultured as described previously (Inaba *et al.*, 1992; Drakes *et al.*, 2006). Briefly, tibias and femurs were harvested from wild-type C57BL/6J mice and cleaned of muscle and tissue. Cleaned bones were rinsed in a 70% ethanol solution and then rinsed with RPMI before bone marrow was harvested. Bone marrow cells were flushed from the bones using a 10-ml syringe of phosphate-buffered saline and an 18-gauge needle. Red blood cells were lysed, and then the tissue suspension was passed through a nylon mesh (9072520; BD Falcon) to remove bone debris. Cells were plated in a 24-well plate at 2×10^6 white blood cells/ml in RPMI culture media (RPMI 1640, 10% FBS, 100 U/ml penicillin/100 U/ml streptomycin, nonessential amino

acids [0.1 mM], sodium pyruvate [1 mM]) supplemented with 7 ng/ml of murine GM-CSF. On day 3 of culture, cell culture media were harvested, spun down, and added back to culture in a 1:1 ratio with fresh media containing 14 ng/ml of GM-CSF. Loosely adherent cells were harvested on day 7 using a sterile plastic pipette. Cells were then seeded on 35-mm glass coverslips, treated with 10 ng/ml of LPS for 12 h, and processed for immunofluorescence as described below.

Lentiviral transduction

Control (sc-108080) and spartin (sc-61602) shRNA lentiviral particles (Santa Cruz Biotechnology) were used according to the manufacturer's protocol. On day 1, RAW264.7 cells were plated at 50% confluence in 12-well plates. The following day (day 2), the medium was removed and replaced with medium containing 5 $\mu\text{g}/\text{ml}$ of polybrene and 30 μl of lentiviral particles. On day 4, the cells were split 1:6, and the next day (day 5), cells were selected for transduction using 6 $\mu\text{g}/\text{ml}$ of puromycin.

Western blotting

Cells were plated on 60-cm dishes and treated with 10 ng/ml of LPS for the indicated times. Cells were then scraped into RIPA buffer (50 mM Tris-HCl, pH 7.5, 150 mM NaCl, 1% NP-40, 0.5% NaDoC, 0.1% sodium deoxycholate, and protease inhibitor cocktail) and lysed by pipetting. Lysates were centrifuged for 10 min at 8000 rpm in a refrigerated (4°C) centrifuge. Supernatants were removed, and 4X Lamella's sample buffer and 2-mercaptoethanol were added to a final concentration of 1X and 715 mM, respectively. Lysates were heated to 100°C for 10 min, loaded, and resolved by SDS-PAGE; this was followed by semidry transfer to nitrocellulose. Blots were then blocked with RapidBlock, probed with the indicated antibodies, and detected using Luminata Forte ECL reagent. Even loading was verified and corrected for by using either β -actin or β -tubulin as a loading control. The intensities of the different bands were quantified using the National Institutes of Health's (NIH) ImageJ gel analysis software.

Confocal immunofluorescence microscopy

Cells were plated on 15-cm glass coverslips and allowed to adhere overnight. After treatment, cells were fixed with 4% paraformaldehyde for 20 min; this was followed by permeabilization with 0.15% Triton-X for 15 min. Cells were then blocked in 5% normal goat serum for 1 h at room temperature and then incubated in primary antibody overnight at 4°C. Secondary antibody incubations were done for 30 min at room temperature, and coverslips were mounted on glass slides using ProLong Gold Antifade Reagent. Images were captured using a Zeiss LSM-510 confocal microscope with a 63 \times /1.4 NA Plan-Apochromat oil-immersion objective at 1024 \times 1024 pixel resolution. Images were processed for publication using Adobe Photoshop.

In experiments using the anti-ubiquitin, Lys-48-Specific-FITC, clone Apu2 antibody, cells were plated, fixed, permeabilized, and blocked as stated above. Primary antibody incubations with anti-spartin and anti-p62 antibody were performed overnight at 4°C and secondary antibody incubations were performed as described. Cells were fixed with 4% paraformaldehyde for 15 min and incubated overnight with the K48-specific antibody at 1:25. Mounting of coverslips was performed as previously stated.

Ubiquitin-binding assays

Pull-down experiments were performed with 4 μg of GST-fusion proteins immobilized on glutathione beads incubated with 0.7 μg of

polyubiquitin chains or monoubiquitin, incubated for 2 h in THG buffer (50 mM HEPES, pH 7.5, 150 mM NaCl, 10% glycerol, and 0.5% Triton X-100), and washed three times. In some experiments, 4–6 µg of GST-fusion proteins cleaved from the GST was incubated with GST-2xUB or GST-4xUB (Bloor *et al.*, 2008). Bound proteins were resolved by SDS-PAGE on a gradient gel followed by semidry transfer to Immobilon-P membrane. Blots were then blocked with RapidBlock solution, probed with the indicated antibodies, and detected using Luminata Forte ECL reagent.

LUMIER assay

Ubiquitin proteins fused to the GST were expressed in *Escherichia coli* and coupled to glutathione beads. For LUMIER assays (Barrios-Rodiles *et al.*, 2005; Bloor *et al.*, 2008), *Renilla* luciferase fused to the full-length WT or spartin mutant III was expressed in HEK293 cells. Twenty-four hours after transfection, cell lysates were incubated with 1xUB, 2xUB, or 4xUB fused to the GST for 2 h in 20 mM Tris-HCl (pH 7.4), 150 mM NaCl, and 0.1% Triton (TNT buffer). Following the incubation, the beads were washed three times, and proteins were eluted with glutathione. The ratio between luciferase activity in eluates versus lysates is presented as fold binding over a control reaction.

NMR spectroscopy

NMR spectra were acquired at 37°C by using a Bruker Avance II 700-MHz NMR spectrometer equipped with an ultrasensitive cryoprobe. For formation of a [U - ^{15}N]ubiquitin complex-WT spartin 155-367, 25 µM of unlabeled WT spartin 155-367 was added to 2.5 µM [U - ^{15}N]ubiquitin dissolved in NMR buffer (90% of 10 mM potassium phosphate [pH 7.0], 100 mM NaCl, 0.02% [wt/vol] NaN_3 , and 10% D_2O). For formation of a [U - ^{15}N]ubiquitin-mutant spartin 155-367 complex, 200 µM of unlabeled mutant spartin 155-367 was added to 10 µM [U - ^{15}N]ubiquitin dissolved in the NMR buffer. For formation of a [U - ^{15}N]spartin 155-367-ubiquitin complex, 50 µM of unlabeled ubiquitin was added to 5 µM of [U - ^{15}N]WT or mutant spartin 155-367 dissolved in the NMR buffer. We used a Watergate version of the 1H { ^{15}N }-edited HSQC (Piotto *et al.*, 1992). Data were recorded with 32 transients as 512×64 complex points in proton and nitrogen dimensions, respectively, apodized with a squared cosine-bell window function, and zero-filled to $1k\{128\}$ data points before Fourier transformation. The corresponding sweep widths were 12 and 35 ppm in the 1H and $\{^{15}N\}$ dimensions, respectively. Chemical shifts of WT spartin 155-367 were assigned by using [U - ^{13}C , ^{15}N]WT spartin 155-367 and a standard suite of triple-resonance experiments (Cavanagh *et al.*, 2007). All spectra were processed using TopSpin, version 2.1 (Bruker), and the assignments were made using Computer Aided Resonance Assignment (CARA; Masse and Keller, 2005). The changes in chemical shifts of amide nitrogens and covalently attached amide protons, $\Delta\Omega$, were calculated by using $\Delta\Omega = [\delta_H^2 + (\delta_N/4)^2]^{1/2}$, where $\delta_{H(N)}$ represents the change in hydrogen and nitrogen chemical shifts (ppm), respectively; $\sqrt{(\Delta\Omega_{NH})^2 + (0.25 \times \Delta\Omega_N)^2}$. Because the HSQC peaks of side-chain amide protons and nitrogens of [U - ^{15}N]WT spartin 155-367 or ubiquitin glutamines do not change position or broaden during complex formation, we used the intensity of the glutamine peak (I_{ref}) to scale the intensities of backbone amide protons and nitrogens. Changes in intensity were calculated by using $\Delta I = (I/I_{ref})_{free} - (I/I_{ref})_{bound}/(I/I_{ref})_{free}$, where I_{free} is the intensity of an individual peak in the in-cell spectrum of free WT spartin 155-367 or ubiquitin, and I_{bound} is the intensity of individual peaks in the NMR spectrum of the WT spartin 155-367-ubiquitin complex. Positive

changes in relative intensities denote peak broadening due to binding interactions (Figure 4; $(I/I_{high})_{control} - (I/I_{high})_{complex}$).

ACKNOWLEDGMENTS

We are grateful to Maureen Drakes (Loyola University Chicago Medical School) for advice and guidance on BMDC cultures. We also thank Marek Tribus and Tim Truong for technical assistance at the bench and in preparation of the manuscript. We thank Rosa Puertollano (National Institute of Diabetes and Digestive and Kidney Diseases, NIH) for valuable suggestions provided to improve the manuscript. This work was supported by the NIH (1R01NS073967-01A1).

REFERENCES

- Amor S, Puentes F, Baker D, van der Valk P (2010). Inflammation in neurodegenerative diseases. *Immunology* 129, 154–169.
- Bakowska JC, Jupille H, Fatheddin P, Puertollano R, Blackstone C (2007). Troyer syndrome protein spartin is mono-ubiquitinated and functions in EGF receptor trafficking. *Mol Biol Cell* 18, 1683–1692.
- Bakowska JC, Wang H, Xin B, Sumner CJ, Blackstone C (2008). Lack of spartin protein in Troyer syndrome: a loss-of-function disease mechanism? *Arch Neurol* 65, 520–524.
- Barrios-Rodiles M *et al.* (2005). High-throughput mapping of a dynamic signaling network in mammalian cells. *Science* 307, 1621–1625.
- Blackstone C (2012). Cellular pathways of hereditary spastic paraplegia. *Annu Rev Neurosci* 35, 25–47.
- Bloor S, Ryzhakov G, Wagner S, Butler PJ, Smith DL, Krumbach R, Dikic I, Randow F (2008). Signal processing by its coil zipper domain activates IKK γ . *Proc Natl Acad Sci USA* 105, 1279–1284.
- Burz DS, Dutta K, Cowburn D, Shekhtman A (2006). Mapping structural interactions using in-cell NMR spectroscopy (STINT-NMR). *Nat Methods* 3, 91–93.
- Burz DS, Shekhtman A (2008). In-cell biochemistry using NMR spectroscopy. *PLoS One* 3, e2571.
- Canadien V, Tan T, Zilber R, Szeto J, Perrin AJ, Brumell JH (2005). Cutting edge: microbial products elicit formation of dendritic cell aggresome-like induced structures in macrophages. *J Immunol* 174, 2471–2475.
- Cavanagh JF, Palmer WJ, Rance AG, Skelton M (2007). *Protein NMR Spectroscopy*, 2nd ed., Burlington, MA: Elsevier.
- Cicarelli FD, Proukakis C, Patel H, Cross H, Azam S, Patton MA, Bork P, Crosby AH (2003). The identification of a conserved domain in both spartin and spastin, mutated in hereditary spastic paraplegia. *Genomics* 81, 437–441.
- Dikic I, Wakatsuki S, Walters KJ (2009). Ubiquitin-binding domains—from structures to functions. *Nat Rev Mol Cell Biol* 10, 659–671.
- Drakes ML, Czinn SJ, Blanchard TG (2006). Regulation of murine dendritic cell immune responses by *Helicobacter felis* antigen. *Infect Immun* 74, 4624–4633.
- Fujita K, Maeda D, Xiao Q, Srinivasula SM (2011). Nrf2-mediated induction of p62 controls Toll-like receptor-4-driven aggresome-like induced structure formation and autophagic degradation. *Proc Natl Acad Sci USA* 108, 1427–1432.
- Hicke L, Schubert HL, Hill CP (2005). Ubiquitin-binding domains. *Nat Rev Mol Cell Biol* 6, 610–621.
- Hirano S, Kawasaki M, Ura H, Kato R, Raiborg C, Stenmark H, Wakatsuki S (2006). Double-sided ubiquitin binding of Hrs-UIM in endosomal protein sorting. *Nat Struct Mol Biol* 13, 272–277.
- Hooper C, Puttamadappa SS, Loring Z, Shekhtman A, Bakowska JC (2010). Spartin activates atrophin-1-interacting protein 4 (AIP4) E3 ubiquitin ligase and promotes ubiquitination of adipophilin on lipid droplets. *BMC Biol* 72-7007-8-72.
- Husebye H, Halaas O, Stenmark H, Tunheim G, Sandanger O, Bogen B, Brech A, Latz E, Espevik T (2006). Endocytic pathways regulate Toll-like receptor 4 signaling and link innate and adaptive immunity. *EMBO J* 25, 683–692.
- Husnjak K, Dikic I (2012). Ubiquitin-binding proteins: decoders of ubiquitin-mediated cellular functions. *Annu Rev Biochem* 81, 291–322.
- Husnjak K, Elsasser S, Zhang N, Chen X, Randles L, Shi Y, Hofmann K, Walters KJ, Finley D, Dikic I (2008). Proteasome subunit Rpn13 is a novel ubiquitin receptor. *Nature* 453, 481–488.
- Inaba K, Inaba M, Romani N, Aya H, Deguchi M, Ikehara S, Muramatsu S, Steinman RM (1992). Generation of large numbers of dendritic cells

- from mouse bone marrow cultures supplemented with granulocyte/macrophage colony-stimulating factor. *J Exp Med* 176, 1693–1702.
- Joshi DC, Bakowska JC (2011). SPG20 protein spartin associates with cardiolipin via its plant-related senescence domain and regulates mitochondrial Ca^{2+} homeostasis. *PLoS One* 6, e19290.
- Kettern N, Rogon C, Limmer A, Schild H, Hohfeld J (2011). The Hsc/Hsp70 co-chaperone network controls antigen aggregation and presentation during maturation of professional antigen presenting cells. *PLoS One* 6, e16398.
- Lehnardt S (2010). Innate immunity and neuroinflammation in the CNS: the role of microglia in Toll-like receptor-mediated neuronal injury. *Glia* 58, 253–263.
- Lelouard H, Ferrand V, Marguet D, Bania J, Camosseto V, David A, Gatti E, Pierre P (2004). Dendritic cell aggresome-like induced structures are dedicated areas for ubiquitination and storage of newly synthesized defective proteins. *J Cell Biol* 164, 667–675.
- Lelouard H, Gatti E, Cappello F, Gresser O, Camosseto V, Pierre P (2002). Transient aggregation of ubiquitinated proteins during dendritic cell maturation. *Nature* 6885, 177–182.
- Manzini MC (2010). Developmental and degenerative features in a complicated spastic paraplegia. *Ann Neurol* 67, 516–525.
- Masse JE, Keller R (2005). AutoLink: automated sequential resonance assignment of biopolymers from NMR data by relative-hypothesis-prioritization-based simulated logic. *J Magn Reson* 174, 133–151.
- Matsuo H, Walters KJ, Teruya K, Tanaka T, Gassner GT, Lippard SJ, Kyogoku Y, Wagner G (1999). Identification by NMR spectroscopy of residues at contact surfaces in large, slowly exchanging macromolecular complexes. *J Am Chem Soc* 121, 9903–9904.
- Nguyen MD, D'Aigle T, Gowing G, Julien JP, Rivest S (2004). Exacerbation of motor neuron disease by chronic stimulation of innate immunity in a mouse model of amyotrophic lateral sclerosis. *J Neurosci* 24, 1340–1349.
- Okun E, Griffioen KJ, Mattson MP (2011). Toll-like receptor signaling in neural plasticity and disease. *Trends Neurosci* 34, 269–281.
- Patel H, Cross H, Proukakis C, Hershberger R, Bork P, Ciccarelli FD, Patton MA, McKusick VA, Crosby AH (2002). SPG20 is mutated in Troyer syndrome, an hereditary spastic paraplegia. *Nat Genet* 31, 347–348.
- Pierre P (2005). Dendritic cells, DRiPs, and DALIS in the control of antigen processing. *Immunol Rev* 207, 184–190.
- Pietrosevoli N, Pancsa R, Tompa P (2013). Structural disorder provides increased adaptability for vesicle trafficking pathways. *PLoS Comput Biol* 9, e1003144.
- Piotto M, Saudek V, Sklenar V (1992). Gradient-tailored excitation for single-quantum NMR spectroscopy of aqueous solutions. *J Biomol NMR* 2, 661–665.
- Polo S, Confalonieri S, Salcini AE, Di Fiore PP (2003). EH and UIM: endocytosis and more. *Sci STKE* 2003, re17.
- Renvoise B, Parker RL, Yang D, Bakowska JC, Hurley JH, Blackstone C (2010). SPG20 protein spartin is recruited to midbodies by ESCRT-III protein Ist1 and participates in cytokinesis. *Mol Biol Cell* 21, 3293–3303.
- Salinas S, Proukakis C, Crosby A, Warner TT (2008). Hereditary spastic paraplegia: clinical features and pathogenetic mechanisms. *Lancet Neurol* 7, 1127–1138.
- Schreiner P, Chen X, Husnjak K, Randles L, Zhang N, Elsasser S, Finley D, Dikic I, Walters KJ, Groll M (2008). Ubiquitin docking at the proteasome through a novel pleckstrin-homology domain interaction. *Nature* 453, 548–552.
- Shekhtman A, Cowburn D (2002). A ubiquitin-interacting motif from Hrs binds to and occludes the ubiquitin surface necessary for polyubiquitination in monoubiquitinated proteins. *Biochem Biophys Res Commun* 296, 1222–1227.
- Sundquist WI, Schubert HL, Kelly BN, Hill GC, Holton JM, Hill CP (2004). Ubiquitin recognition by the human TSG101 protein. *Mol Cell* 13, 783–789.
- Teo H, Vepintsev DB, Williams RL (2004). Structural insights into endosomal sorting complex required for transport (ESCRT-I) recognition of ubiquitinated proteins. *J Biol Chem* 279, 28689–28696.
- Urbanczyk A, Enz R (2011). Spartin recruits PKC- ζ via the PKC- ζ -interacting proteins ZIP1 and ZIP3 to lipid droplets. *J Neurochem* 118, 737–748.
- Wishart DS, Sykes BD (1994). The ^{13}C chemical-shift index: a simple method for the identification of protein secondary structure using ^{13}C chemical-shift data. *J Biomol NMR* 4, 171–180.
- Xie J, Burz DS, He W, Bronstein IB, Lednev I, Shekhtman A (2007). Hexameric calgranulin C (S100A12) binds to the receptor for advanced glycosylated end products (RAGE) using symmetric hydrophobic target-binding patches. *J Biol Chem* 282, 4218–4231.
- Yewdell JW, Schubert U, Binnik JR (2001). At the crossroads of cell biology and immunology: DRiPs and other sources of peptide ligands for MHC class I molecules. *J Cell Sci Pt* 114, 845–851.
- Zuiderweg ER (2002). Mapping protein-protein interactions in solution by NMR spectroscopy. *Biochemistry* 41, 1–7.